

Effect of hydrostatic pressure and longitudinal electric field on phase transitions and thermodynamic characteristics of quasione-dimensional CsH_2PO_4 ferroelectric

A.S. Vdovych¹, I.R. Zachek², R.R. Levitskii¹

¹ Institute for Condensed Matter Physics of the National Academy of Sciences of Ukraine,
1 Svientsitskii St., 79011 Lviv, Ukraine

² Lviv Polytechnic National University, 1 S. Bandera St., 79013, Lviv, Ukraine

Received December 12, 2019, in final form March 9, 2020

We propose a two-sublattice proton ordering model for the quasione-dimensional CsH_2PO_4 ferroelectric with hydrogen bonds, which takes into account linear on lattice strains u_1 , u_2 , u_3 and u_5 contribution to the energy of proton subsystem. The model also takes into account the dependence of effective dipole moments of pseudospins on the order parameters, which enables one to agree the effective dipole moments in paraelectric and ferroelectric phases. Within this model in two-particle cluster approximation on short-range interactions and in the mean field approximation on long-range interactions, there is investigated the behaviour of spontaneous polarization, longitudinal dielectric permittivity and molar heat capacity under the action of hydrostatic pressure and longitudinal electric field. The phase transition into antiferroelectric phase under high pressures is explained. The character of smearing of the paraelectric-ferroelectric phase transition as well as suppression of the antiferroelectric phase at the presence of electric field is studied.

Key words: *ferroelectrics, phase transitions, dielectric permittivity, hydrostatic pressure effect, electric field effect*

1. Introduction

Investigations of the pressure and field effects on physical properties of ferroelectrics are urgent indeed because they make it possible to deeper understand the mechanisms of phase transitions in these materials as well as to carry out a search for the new physical effects, which are not observed under zero pressure and zero external field.

A ferroelectric with hydrogen bonds CsH_2PO_4 (CDP) is an example of the crystal where the pressure and field effects are essential. In this crystal there are two structurally inequivalent types of hydrogen bonds of different length (figure 1 a). Longer bonds have one equilibrium position for protons, whereas shorter bonds have two equilibrium positions. They link PO_4 groups into chains along b -axis (figure 1 b); therefore, the crystal is quasione-dimentional. At room temperature and under zero pressure, the crystal is in the paraelectric phase and has a monoclinic symmetry (space group $\text{P2}_1/\text{m}$) [1, 2]. In this case, protons on the shorter bonds occupy two equilibrium positions with equal probability. Below $T_c = 153$ K, the crystal passes into the ferroelectric phase (space group P2_1) [3, 4] with spontaneous polarization along crystallographic b -axis, and the protons occupy mainly the upper equilibrium position (figure 1, b).

Based on dielectric investigations [5, 6], it was determined that under pressure $p_c = 0.33$ GPa and $T_c^{\text{cr}} = 124.6$ K, there appear double hysteresis loops, which means that the crystal passes to the antiferroelectric phase. Using investigations on neutron scattering [7], it was established that in the antiferroelectric phase a primitive cell of CDP crystal redoubles along a -axis, because there appear two sublattices in the form of (b,c) -planes, which are polarized antiparallely along b -axis and alternate along

a -axis. Symmetry of the crystal remains monoclinic (space group $P2_1$), and parameters of the redoubled lattice are as follows: $a = 15.625 \text{ \AA}$, $b = 6.254 \text{ \AA}$, $c = 4.886 \text{ \AA}$, $\beta = 108.08^\circ$. Thus, there takes place a quite large shift of Cs atoms and PO_4 groups in (a, c) -plane and the rotation of the PO_4 groups by 36.8° around b -axis, which passes through P atom. The protons on the hydrogen bonds of the neighbour sublattices are ordered antiparallely. Under very high pressures, there appears a new antiferroelectric phase (AF2), where two sublattices have the form of chains along b -axis, which are polarized antiparallely along b -axis and have a checkerboard arrangement. The phase AF2 was predicted in [8] based on the NMR investigations and was confirmed in [9] on the basis of dielectric constant measurements at low temperature and X-ray diffraction measurements.

Results of dielectric constant measurements under hydrostatic pressure, presented in [6, 9–11], do not agree with each other. In particular, there are different rates of change of the phase transition temperature with pressure, as well as different maximum values of dielectric permittivity. This is indicative of high sensitivity of the dielectric properties to the quality of the grown samples of CDP.

An attempt to theoretically describe the paraelectric-ferroelectric and paraelectric-antiferroelectric phase transition in CsH_2PO_4 and CsD_2PO_4 as well as experimental data for the dielectric permittivity was made in [12], where the crystal is described as pseudospin Ising chains. The interactions between the pseudospins within a chain are taken into account strictly, whereas the dipole-dipole interactions between the pseudospins of different chains are determined in the mean field approximation. Therein, expressions for spontaneous polarization and dielectric permittivity and equations for the phase transition temperatures were obtained. It was considered that the interactions linearly decrease with pressure, while the interchain interactions change their sign under the pressure higher than the critical value. However, there was not examined the issue about a description of the experimental data for dielectric constant by the proposed theory.

Later on, in [13] using the pseudospin model [12] and the two-particle cluster approximation for short-range configuration interactions, there were calculated thermodynamic and dynamic characteristics of CDP type ferroelectrics at different values of hydrostatic pressure. A good agreement of the theory with the experimental data for the dielectric constant and for pressure dependence of the para-ferroelectric and para-antiferroelectric phase transition temperatures was obtained. However, in the model [12, 13], one cannot calculate piezoelectric and elastic characteristics of the crystal, and the critical pressure does not depend on temperature.

In [14], temperature dependences of the lattice strains u_1 , u_2 , u_3 , u_5 were measured. There was also proposed a quasione-dimensional Ising model for CDP crystal, where the parameters of interaction are linear functions of these strains. Based on this model, the temperature dependences $u_j(T)$ were explained. However, this model does not consider the crystal as two sublattices and does not enable one to describe the ferroelectric-antiferroelectric phase transition under high pressures.

In [15], there was proposed a two-sublattice model of compressible CDP crystal, where the interactions between the neighbouring pseudospins within a chain are taken into account in the two-particle cluster approximation, whereas long-range (including interchain) interactions — in the mean field approximation. Here, interaction parameters are linear functions of strains u_j . As a result, there were calculated the temperature dependences of spontaneous polarization, dielectric permittivity, piezoelectric coefficients and elastic constants.

In [16], using the proposed in [15] model of deformed CDP crystal, there was investigated the effect of hydrostatic pressure on the phase transition temperature, longitudinal static dielectric characteristics of $\text{Cs}(\text{H}_{1-x}\text{D}_x)_2\text{PO}_4$ crystals.

As it is well known, at the presence of the longitudinal field E_y , a second order phase transition smears, and the temperature dependence of the longitudinal permittivity $\varepsilon_{yy}(T)$ shows a rounded maximum. At the same time, in [15, 16], the effective dipole moments, which have different values in the paraelectric and ferroelectric phases, were used to calculate the longitudinal dielectric permittivity ε_{yy} . This leads to the appearance of a break on the curve $\varepsilon_{yy}(T)$ instead of the rounded maximum at the presence of the external field E_y . Therefore, in order to describe the smearing of the phase transition, in the present paper we modified the model [15] assuming that the effective dipole moment on a hydrogen bond depends on the order parameter on this bond because the order parameter depends on temperature continuously near the phase transition point.

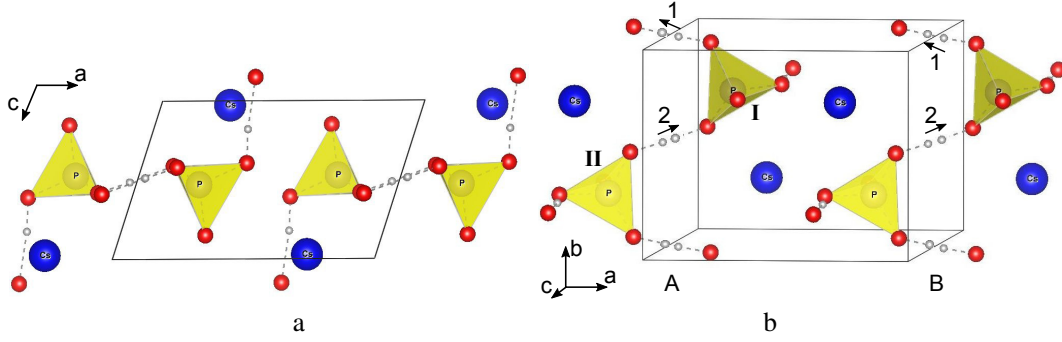


Figure 1. (Colour online) Primitive cell of CsH_2PO_4 crystal in the ferroelectric phase.

2. The model of CDP crystal

We consider the system of protons in CDP, localized on short $\text{O-H}\dots\text{O}$ bonds between the groups PO_4 , which form zigzag chains along the crystallographic b -axis of the crystal (see figure 1). The primitive cell includes one chain, marked as “A” in figure 1. Further, we consider the restricted primitive cell, which includes two chains (“A” and “B”) in order to describe the transition to the antiferroelectric phase under high pressure. All the chains “A” form a sublattice “A”, whereas all the chains “B” form a sublattice “B”. Every chain in the primitive cell includes two neighbouring tetrahedra PO_4 (of type “I” and “II”) together with two short hydrogen bonds (respectively, “1” and “2”).

Dipole moments $\vec{d}_{q1}^A, \vec{d}_{q2}^A, \vec{d}_{q1}^B, \vec{d}_{q2}^B$, are ascribed to the protons on the bonds. Pseudospin variables $\frac{\sigma_{q1}^A}{2}, \frac{\sigma_{q2}^A}{2}, \frac{\sigma_{q1}^B}{2}, \frac{\sigma_{q2}^B}{2}$ describe reorientation of the respective dipole moments of the base units: $\vec{d}_{q1,2}^{A,B} = \vec{\mu}_{q1,2}^{A,B} \frac{\sigma_{q1,2}^{A,B}}{2}$. Mean values $\langle \frac{\sigma}{2} \rangle = \frac{1}{2}(n_a - n_b)$ are connected with differences in occupancy of the two possible molecular positions, n_a and n_b .

Hamiltonian of proton subsystem of CDP takes into account short-range and long-range interactions. Under the stresses maintaining the symmetry of crystal $\sigma_1 = \sigma_{xx}, \sigma_2 = \sigma_{yy}, \sigma_3 = \sigma_{zz}, \sigma_5 = \sigma_{xz}$ ($X \perp (b,c), Y \parallel b, Z \parallel c$), and in the presence of electric field $E_2 = E_y$, it can be written in such a way:

$$\hat{H} = N U_{\text{seed}} + \hat{H}_{\text{short}} + \hat{H}_{\text{long}} + \hat{H}_E + \hat{H}'_E, \quad (2.1)$$

where N is the total number of restricted primitive cells.

The first term in (2.1) is “seed” energy, which relates to the heavy ion sublattice and does not explicitly depend on the configuration of the proton subsystem. It includes elastic, piezoelectric and dielectric parts, expressed in terms of the electric field E_2 and strains maintaining the symmetry of crystal $u_1 = u_{xx}, u_2 = u_{yy}, u_3 = u_{zz}, u_5 = 2u_{xz}$:

$$U_{\text{seed}} = v \left(\frac{1}{2} \sum_{j,j'} c_{jj'}^{E0} u_j u_{j'} - \sum_j e_{2j}^0 E_2 u_j - \frac{1}{2} \chi_{22}^{u0} E_2^2 \right), \quad j, j' = 1, 2, 3, 5. \quad (2.2)$$

Parameters $c_{jj'}^{E0}, e_{2j}^0, \chi_{22}^{u0}$ are the so-called “seed” elastic constants, “seed” coefficients of piezoelectric stresses and “seed” dielectric susceptibility, respectively; v is the volume of a restricted primitive cell. In the paraelectric phase all coefficients $e_{ij}^0 \equiv 0$.

Other terms in (2.1) describe the pseudospin part of Hamiltonian. In particular, the second term in (2.1) is Hamiltonian of short-range interactions:

$$\hat{H}_{\text{short}} = -2w \sum_{qq'} \left(\frac{\sigma_{q1}^A}{2} \frac{\sigma_{q'2}^A}{2} + \frac{\sigma_{q1}^B}{2} \frac{\sigma_{q'2}^B}{2} \right) (\delta_{\mathbf{R}_q \mathbf{R}_{q'}} + \delta_{\mathbf{R}_q + \mathbf{R}_b, \mathbf{R}_{q'}}). \quad (2.3)$$

In (2.3), $\sigma_{q1,2}^{A,B}$ are z -components of pseudospin operator that describe the state of the bond “1” or “2” of the chain “A” or “B”, in the q -th cell, \mathbf{R}_b is the lattice vector along OY-axis. The first Kronecker delta corresponds to the interaction between protons in the chains near the tetrahedra PO_4 of type “I”, where the second Kronecker delta corresponds to the interaction near the tetrahedra PO_4 of type “II”. Contributions into the energy of interactions between pseudospins near tetrahedra of different type are identical.

Parameter w , which describes the short-range interactions within the chains, is expanded linearly into a series with respect to strains u_j :

$$w = w^0 + \sum_j \delta_{2j} u_j, \quad (j = 1, 2, 3, 5). \quad (2.4)$$

The term \hat{H}_{long} in (2.1) describes long-range dipole-dipole interactions and indirect (i.e., through the lattice vibrations) interactions between protons which are taken into account in the mean field approximation:

$$\begin{aligned} \hat{H}_{\text{long}} = & \frac{1}{2} \sum_{\substack{qq' \\ ff'}} J_{ff'}(qq') \frac{\langle \sigma_{qf}^A \rangle}{2} \frac{\langle \sigma_{q'f'}^A \rangle}{2} - \sum_{\substack{qq' \\ ff'}} J_{ff'}(qq') \frac{\langle \sigma_{q'f'}^A \rangle}{2} \frac{\sigma_{qf}^A}{2} \\ & + \frac{1}{2} \sum_{\substack{qq' \\ ff'}} J_{ff'}(qq') \frac{\langle \sigma_{qf}^B \rangle}{2} \frac{\langle \sigma_{q'f'}^B \rangle}{2} - \sum_{\substack{qq' \\ ff'}} J_{ff'}(qq') \frac{\langle \sigma_{q'f'}^B \rangle}{2} \frac{\sigma_{qf}^B}{2} \\ & + \frac{1}{2} \sum_{\substack{qq' \\ ff'}} K_{ff'}(qq') \frac{\langle \sigma_{qf}^A \rangle}{2} \frac{\langle \sigma_{q'f'}^B \rangle}{2} - \sum_{\substack{qq' \\ ff'}} K_{ff'}(qq') \frac{\langle \sigma_{q'f'}^B \rangle}{2} \frac{\sigma_{qf}^A}{2} \\ & + \frac{1}{2} \sum_{\substack{qq' \\ ff'}} K_{ff'}(qq') \frac{\langle \sigma_{qf}^B \rangle}{2} \frac{\langle \sigma_{q'f'}^A \rangle}{2} - \sum_{\substack{qq' \\ ff'}} K_{ff'}(qq') \frac{\langle \sigma_{q'f'}^A \rangle}{2} \frac{\sigma_{qf}^B}{2}, \end{aligned} \quad (2.5)$$

where the first two terms describe the effective long-range interaction between pseudospins within the same sublattice “A” or “B”, whereas two other terms — between pseudospins of different sublattices “A” and “B”. Taking into account that $\langle \sigma_{qf}^{A,B} \rangle$ does not depend on the number of primitive cells q , we write (2.5) in such a way:

$$\hat{H}_{\text{long}} = NH^0 + \hat{H}_2, \quad (2.6)$$

where

$$\begin{aligned} H^0 = & \frac{1}{8} \left[J_{11} \left(\langle \sigma_1^A \rangle^2 + \langle \sigma_1^B \rangle^2 \right) + J_{22} \left(\langle \sigma_2^A \rangle^2 + \langle \sigma_2^B \rangle^2 \right) + 2J_{12} \left(\langle \sigma_1^A \rangle \langle \sigma_2^A \rangle + \langle \sigma_1^B \rangle \langle \sigma_2^B \rangle \right) \right] \\ & + \frac{1}{4} \left[K_{11} \langle \sigma_1^A \rangle \langle \sigma_1^B \rangle + K_{22} \langle \sigma_2^A \rangle \langle \sigma_2^B \rangle + K_{12} \left(\langle \sigma_1^A \rangle \langle \sigma_2^B \rangle + \langle \sigma_1^B \rangle \langle \sigma_2^A \rangle \right) \right], \end{aligned} \quad (2.7)$$

$$\begin{aligned} \hat{H}_2 = & - \sum_q \left\{ \left(J_{11} \langle \sigma_1^A \rangle + J_{12} \langle \sigma_2^A \rangle + K_{11} \langle \sigma_1^B \rangle + K_{12} \langle \sigma_2^B \rangle \right) \frac{\sigma_{q1}^A}{4} \right. \\ & + \left(J_{12} \langle \sigma_1^A \rangle + J_{22} \langle \sigma_2^A \rangle + K_{12} \langle \sigma_1^B \rangle + K_{22} \langle \sigma_2^B \rangle \right) \frac{\sigma_{q2}^A}{4} \\ & + \left(J_{11} \langle \sigma_1^B \rangle + J_{12} \langle \sigma_2^B \rangle + K_{11} \langle \sigma_1^A \rangle + K_{12} \langle \sigma_2^A \rangle \right) \frac{\sigma_{q1}^B}{4} \\ & \left. + \left(J_{12} \langle \sigma_1^B \rangle + J_{22} \langle \sigma_2^B \rangle + K_{12} \langle \sigma_1^A \rangle + K_{22} \langle \sigma_2^A \rangle \right) \frac{\sigma_{q2}^B}{4} \right\}. \end{aligned} \quad (2.8)$$

Here, parameters $J_{ff'} = \sum_{\mathbf{R}_q - \mathbf{R}_{q'}} J_{ff'}(qq')$ and $K_{ff'} = \sum_{\mathbf{R}_q - \mathbf{R}_{q'}} K_{ff'}(qq')$ are Fourier transforms of long-range interaction constants at $\mathbf{k} = 0$. The parameters $J_{ff'}$ and $K_{ff'}$ are expanded linearly into a series with respect to strains u_j :

$$\begin{aligned} J_{11} = J_{22} = J_1 + \sum_j \bar{\varphi}_{1j} u_j, \quad J_{12} = J_{21} = J_2 + \sum_j \bar{\varphi}_{2j} u_j, \\ K_{11} = K_{22} = K_1 + \sum_j \varphi_{1j} u_j, \quad K_{12} = K_{21} = K_2 + \sum_j \varphi_{2j} u_j. \end{aligned} \quad (2.9)$$

Taking into account such symmetry of pseudospins in the chains of CDP

$$\langle \sigma_{q1}^A \rangle = \langle \sigma_{q2}^A \rangle = \eta_1, \quad \langle \sigma_{q1}^B \rangle = \langle \sigma_{q2}^B \rangle = \eta_2, \quad (2.10)$$

we write expressions (2.7), (2.8) in such a way:

$$\hat{H}^0 = \nu_1(\eta_1^2 + \eta_2^2) + 2\nu_2\eta_1\eta_2, \quad (2.11)$$

$$\hat{H}_2 = \sum_q \left[-(2\nu_1\eta_1 + 2\nu_2\eta_2) \left(\frac{\sigma_{q1}^A}{2} + \frac{\sigma_{q2}^A}{2} \right) - (2\nu_2\eta_1 + 2\nu_1\eta_2) \left(\frac{\sigma_{q1}^B}{2} + \frac{\sigma_{q2}^B}{2} \right) \right]. \quad (2.12)$$

Here, the following notations are used:

$$\nu_1 = \frac{1}{8}(J_{11} + J_{22} + 2J_{12}) = \nu_1^0 + \sum_j \psi_{j1} u_j, \quad \nu_1^0 = \frac{1}{4}(J_1 + J_2), \quad \psi_{j1} = \frac{1}{4}(\bar{\varphi}_{1j} + \varphi_{1j}), \quad (2.13)$$

$$\nu_2 = \frac{1}{8}(K_{11} + K_{22} + 2K_{12}) = \nu_2^0 + \sum_j \psi_{j2} u_j, \quad \nu_2^0 = \frac{1}{4}(K_1 + K_2), \quad \psi_{j2} = \frac{1}{4}(\bar{\varphi}_{2j} + \varphi_{2j}). \quad (2.14)$$

The fourth term in (2.1) describes the interactions of pseudospins with the external electric field:

$$\hat{H}_E = - \sum_q \mu_y E_2 \left(\frac{\sigma_{q1}^A}{2} + \frac{\sigma_{q2}^A}{2} + \frac{\sigma_{q1}^B}{2} + \frac{\sigma_{q2}^B}{2} \right), \quad (2.15)$$

where μ_y is y -component of effective dipole moments per one pseudospin.

The term \hat{H}'_E in Hamiltonian (2.1) takes into account the above mentioned dependence of effective dipole moments on the mean value of pseudospin s_f :

$$\hat{H}'_E = - \sum_{qf} s_f^2 \mu' E_2 \frac{\sigma_{qf}}{2} = - \sum_{qf} \left(\frac{1}{N} \sum_{q'} \sigma_{q'f} \right)^2 \mu' E_2 \frac{\sigma_{qf}}{2}. \quad (2.16)$$

where σ_{qf} ($f=1, 2, 3, 4$) are brief notations of pseudospins σ_{q1}^A , σ_{q2}^A , σ_{q1}^B , σ_{q2}^B , respectively. Here, we use corrections to dipole moments $s_f^2 \mu'$ instead of $s_f \mu'$ due to the symmetry considerations, the energy should not change, when field and all pseudospins change their sign.

The term \hat{H}'_E , as well as long-range interactions, are taken into account in the mean field approximation:

$$\begin{aligned} \hat{H}'_E &= - \sum_{qf} \left(\frac{1}{N} \sum_{q'} \sigma_{q'f} \right)^2 \mu' E_2 \frac{\sigma_{qf}}{2} = - \frac{1}{N^2} \sum_{qf} \sum_{q'} \sum_{q''} \sigma_{qf} \sigma_{q'f} \sigma_{q''f} \frac{\mu' E_2}{2} \\ &\approx - \frac{1}{N^2} \sum_{qf} \sum_{q'} \sum_{q''} \left[(\sigma_{qf} + \sigma_{q'f} + \sigma_{q''f}) \eta_f^2 - 2\eta_f^3 \right] \frac{\mu' E_2}{2} \\ &= -3 \sum_q \sum_{f=1}^4 \frac{\sigma_{qf}}{2} \eta_f^2 \mu' E_2 + N \sum_{f=1}^4 \eta_f^3 \mu' E_2. \end{aligned} \quad (2.17)$$

Taking into account (2.10), expression (2.17) can be written as:

$$\hat{H}'_E = -3 \sum_q \mu' E_2 \left(\frac{\eta_1^2 \sigma_{q1}^A}{2} + \frac{\eta_1^2 \sigma_{q2}^A}{2} + \frac{\eta_2^2 \sigma_{q1}^B}{2} + \frac{\eta_2^2 \sigma_{q2}^B}{2} \right) + 2N(\eta_1^3 + \eta_2^3) \mu' E_2. \quad (2.18)$$

The two-particle cluster approximation for short-range interactions is used to calculate the thermodynamic characteristics of CDP. In this approximation, thermodynamic potential is given by:

$$G = NU_{\text{seed}} + NH^0 + 2N(\eta_1^3 + \eta_2^3) \mu' E_2 - Nv \sum_j \sigma_j u_j - k_B T \sum_q \left\{ 2 \ln \text{Spe}^{-\beta \hat{H}_q^{(2)}} - \ln \text{Spe}^{-\beta \hat{H}_q^{(1)A}} - \ln \text{Spe}^{-\beta \hat{H}_q^{(1)B}} \right\}, \quad (2.19)$$

where $\beta = \frac{1}{k_B T}$, k_B is Boltzmann constant, $\hat{H}_q^{(2)}$, $\hat{H}_q^{(1)A}$, $\hat{H}_q^{(1)B}$ are two-particle and one-particle Hamiltonians:

$$\hat{H}_q^{(2)} = -2w \left(\frac{\sigma_{q1}^A \sigma_{q2}^A}{2} + \frac{\sigma_{q1}^B \sigma_{q2}^B}{2} \right) - \frac{y_1}{\beta} \left(\frac{\sigma_{q1}^A}{2} + \frac{\sigma_{q2}^A}{2} \right) - \frac{y_2}{\beta} \left(\frac{\sigma_{q1}^B}{2} + \frac{\sigma_{q2}^B}{2} \right), \quad (2.20)$$

$$\hat{H}_q^{(1)A} = -\frac{\bar{y}_1}{\beta} \left(\frac{\sigma_{q1}^A}{2} + \frac{\sigma_{q2}^A}{2} \right), \quad \hat{H}_q^{(1)B} = -\frac{\bar{y}_2}{\beta} \left(\frac{\sigma_{q1}^B}{2} + \frac{\sigma_{q2}^B}{2} \right), \quad (2.21)$$

where such notations are used:

$$y_1 = \beta \Delta_1 + 2\beta v_1 \eta_1 + 2\beta v_2 \eta_2 + \beta(\mu_y E_2 + 3\eta_1^2 \mu' E_2), \quad (2.22)$$

$$y_2 = \beta \Delta_2 + 2\beta v_2 \eta_1 + 2\beta v_1 \eta_2 + \beta(\mu_y E_2 + 3\eta_2^2 \mu' E_2), \quad (2.23)$$

$$\bar{y}_1 = \beta \Delta_1 + y_1, \quad \bar{y}_2 = \beta \Delta_2 + y_2.$$

Symbols Δ_l are effective field, created by the neighboring bonds from outside the cluster. In the cluster approximation, these fields can be determined from the condition of minimum of thermodynamic potential $\partial G / \partial \Delta_l = 0$, which gives the self-consistency condition, which states that the mean values of the pseudospins $\langle \sigma_{qf}^{A,B} \rangle$ calculated using two-particle and one-particle Gibbs distribution, respectively, should coincide; that is,

$$\begin{aligned} \eta_1 &= \frac{\text{Sp} \sigma_{qf}^A e^{-\beta \hat{H}_q^{(2)}}}{\text{Sp} e^{-\beta \hat{H}_q^{(2)}}} = \frac{\text{Sp} \sigma_{qf}^A e^{-\beta \hat{H}_q^{(1)A}}}{\text{Sp} e^{-\beta \hat{H}_q^{(1)A}}}, \\ \eta_2 &= \frac{\text{Sp} \sigma_{qf}^B e^{-\beta \hat{H}_q^{(2)}}}{\text{Sp} e^{-\beta \hat{H}_q^{(2)}}} = \frac{\text{Sp} \sigma_{qf}^B e^{-\beta \hat{H}_q^{(1)B}}}{\text{Sp} e^{-\beta \hat{H}_q^{(1)B}}}. \end{aligned} \quad (2.24)$$

Hence, based on (2.24), taking into account (2.10), (2.20) and (2.21), we obtain expressions for the order parameters:

$$\begin{aligned} \eta_1 &= \frac{1}{D} [\sinh(y_1 + y_2) + \sinh(y_1 - y_2) + 2a \sinh y_1] = \tanh \frac{\bar{y}_1}{2}, \\ \eta_2 &= \frac{1}{D} [\sinh(y_1 + y_2) - \sinh(y_1 - y_2) + 2a \sinh y_2] = \tanh \frac{\bar{y}_2}{2}, \end{aligned} \quad (2.25)$$

where such notations are used:

$$D = \cosh(y_1 + y_2) + \cosh(y_1 - y_2) + 2a \cosh y_1 + 2a \cosh y_2 + 2a^2, \\ a = e^{-\frac{w}{k_B T}}.$$

Excluding the cluster fields Δ_l from expression $\eta_l = \tanh(\bar{y}_l/2)$ [see (2.25)], we write (2.22), (2.23) in such a way:

$$y_1 = \frac{1}{2} \ln \frac{1 + \eta_1}{1 - \eta_1} + \beta v_1 \eta_1 + \beta v_2 \eta_2 + \frac{1}{2} \beta \left(\mu_y E_2 + 3\eta_1^2 \mu' E_2 \right), \quad (2.26)$$

$$y_2 = \frac{1}{2} \ln \frac{1 + \eta_2}{1 - \eta_2} + \beta v_2 \eta_1 + \beta v_1 \eta_2 + \frac{1}{2} \beta \left(\mu_y E_2 + 3\eta_2^2 \mu' E_2 \right). \quad (2.27)$$

3. Longitudinal dielectric and thermal characteristics of CDP

Using (2.19), thermodynamic potential per one restricted primitive cell can be written in such a way:

$$\begin{aligned} g &= U_{\text{seed}} + H^0 + 2 \left(\eta_1^3 + \eta_2^3 \right) \mu' E_2 + 2k_B T \ln 2 - 2w - v \sum_j \sigma_j u_j \\ &- k_B T \ln \left(1 - \eta_1^2 \right) - k_B T \ln \left(1 - \eta_2^2 \right) - 2k_B T \ln D. \end{aligned} \quad (3.1)$$

Using equilibrium condition

$$\left(\frac{\partial g}{\partial u_j} \right)_{E_2} = 0,$$

we obtain equations for strains u_j :

$$\sigma_j = c_{j1}^{E0} u_1 + c_{j2}^{E0} u_2 + c_{j3}^{E0} u_3 + c_{j5}^{E0} u_5 - e_{2j}^0 E_2 - \frac{2\delta_j}{v} + \frac{4\delta_j}{vD} M - \frac{1}{v} \psi_{j1} (\eta_1^2 + \eta_2^2) - \frac{2}{v} \psi_{j2} \eta_1 \eta_2, \quad (3.2)$$

where

$$M = [a \cosh y_1 + a \cosh y_2 + 2a^2].$$

In the case of applying the hydrostatic pressure $\sigma_1 = \sigma_2 = \sigma_3 = -p$, $\sigma_4 = \sigma_5 = \sigma_6 = 0$.

Based on thermodynamic potential (3.1), we get expressions for different thermodynamic characteristics. In particular, an expression for longitudinal polarization P_2 :

$$P_2 = - \left(\frac{\partial g}{\partial E_2} \right)_{\sigma_j} = \sum_j e_{2j}^0 u_j + \chi_{22}^{u0} E_2 + \frac{\mu_y}{v} (\eta_1 + \eta_2) + \frac{\mu'}{v} (\eta_1^3 + \eta_2^3). \quad (3.3)$$

Isothermic dielectric susceptibility of a mechanically clamped crystal is given by:

$$\begin{aligned} \chi_{22}^u &= \left(\frac{\partial P_2}{\partial E_2} \right)_{u_j} = \chi_{22}^{u0} + \frac{\beta \tilde{\mu}_{1y}^2}{2v\Delta} [D(\kappa_{11} + \kappa_{12}) - (\tilde{\varphi}_2 - \beta v_2)(\kappa_{11}\kappa_{22} - \kappa_{12}^2)] \\ &+ \frac{\beta \tilde{\mu}_{2y}^2}{2v\Delta} [D(\kappa_{12} + \kappa_{22}) - (\tilde{\varphi}_1 - \beta v_2)(\kappa_{11}\kappa_{22} - \kappa_{12}^2)], \end{aligned} \quad (3.4)$$

with the following notations:

$$\Delta = D^2 - D [\tilde{\varphi}_1 \kappa_{11} + \tilde{\varphi}_2 \kappa_{22} + 2\beta v_2 \kappa_{12}] + [\tilde{\varphi}_1 \tilde{\varphi}_2 - (\beta v_2)^2] (\kappa_{11}\kappa_{22} - \kappa_{12}^2),$$

$$\tilde{\varphi}_1 = \varphi_1 + 3\eta_1 \beta \mu' E_2, \quad \tilde{\varphi}_2 = \varphi_2 + 3\eta_2 \beta \mu' E_2,$$

$$\varphi_1 = \frac{1}{1 - \eta_1^2} + \beta v_1, \quad \varphi_2 = \frac{1}{1 - \eta_2^2} + \beta v_2,$$

$$\tilde{\mu}_{1y} = \mu_y + 3\mu' \eta_1^2, \quad \tilde{\mu}_{2y} = \mu_y + 3\mu' \eta_2^2,$$

$$\begin{aligned}
\kappa_{11} &= \cosh(y_1 + y_2) + \cosh(y_1 - y_2) + 2a \cosh y_1 - \eta_1^2 D, \\
\kappa_{12} &= \cosh(y_1 + y_2) - \cosh(y_1 - y_2) - \eta_1 \eta_2 D, \\
\kappa_{21} &= \cosh(y_1 + y_2) - a^2 \cosh(y_1 - y_2) + 2a \cosh y_2 - \eta_1 \eta_2 D, \\
\kappa_{22} &= \cosh(y_1 + y_2) + \cosh(y_1 - y_2) + 2a \cosh y_2 - \eta_2^2 D.
\end{aligned}$$

Molar heat capacity of the proton subsystem of CDP at a constant pressure can be found by numerical differentiation of thermodynamic potential:

$$\Delta C_p = -\frac{N_A T}{4} \left(\frac{\partial^2 g}{\partial T^2} \right)_{\sigma_j} . \quad (3.5)$$

where N_A is the Avogadro constant.

4. Comparison of theoretical results with the experimental data. Discussion.

The theory parameters are determined from the condition of agreement of the calculated characteristics with experimental data for temperature dependences of spontaneous polarization $P_2(T)$ and dielectric permittivity $\varepsilon_{22}(T)$ at different values of hydrostatic pressure [6], spontaneous strains u_j [14], molar heat capacity [17] and elastic constants [18]; as well as the agreement with ab-initio calculations of the lattice contributions to molar heat capacity [19] and dielectric permittivity [20].

Parameters of short-range interactions w_0 and long-range interactions v_1^0 (“intra-sublattice”), v_2^0 (“inter-sublattice”) mainly fix the phase transition temperature from paraelectric to ferroelectric phase at the absence of external pressure and field, the order of phase transition and the shape of curve $P_2(T)$. Their optimal values are: $w_0/k_B=650$ K, $v_1^0/k_B=1.50$ K, $v_2^0/k_B=0.23$ K.

To determine the deformational potentials δ_j [see(2.4)] and ψ_{j1} (2.13), ψ_{j2} (2.13) it is necessary to use experimental data for shift of the phase transition temperature under hydrostatic and uniaxial pressures as well as the data for temperature dependences of spontaneous strains u_j , piezoelectric coefficients and elastic constants. Unfortunately, only data for spontaneous strains and hydrostatic pressure effect on the dielectric characteristics are available. As a result, the experimental data for strains and dielectric characteristics can be described using a great number of combinations of parameters ψ_{j1} , ψ_{j2} . Therefore, for the sake of simplicity, we chose ψ_{j2} to be proportional to ψ_{j1} . Optimal values of deformational potentials are: $\delta_1/k_B = 1214$ K, $\delta_2/k_B = 454$ K, $\delta_3/k_B = 1728$ K, $\delta_5/k_B = 1214$ K, $\delta_5/k_B = -13$ K; $\psi_{11}/k_B = 92.2$ K, $\psi_{21}/k_B = 23.2$ K, $\psi_{31}/k_B = 139.7$ K, $\psi_{51}/k_B = 5.5$ K; $\psi_{j2} = \frac{1}{3}\psi_{j1}$.

The effective dipole moment in the paraelectric phase is found from the condition of agreement of calculated curve $\varepsilon_{22}(T)$ with experimental data. We consider it to be dependent on the value of hydrostatic pressure p , that is $\mu_y = \mu_y^0(1 - k_p p)$, where $\mu_y^0 = 2.63 \cdot 10^{-18}$ esu·cm, $k_p = 0.4 \cdot 10^{-10}$ cm²/dyn. The correction to the effective dipole moment $\mu' = -0.43 \cdot 10^{-18}$ esu·cm is found from the condition of agreement of the calculated saturation polarization with experimental data.

The “seed” dielectric susceptibility χ_{22}^{u0} , coefficients of piezoelectric stress e_{2j}^0 and elastic constants c_{ij}^{E0} are found from the condition of agreement of theory with experimental data in the temperature regions far from the phase transition temperature T_c . Their values are obtained as follows: $\chi_{22}^{u0} = 0.443$ [20]; $e_{2j}^0 = 0$ esu/cm²; $c_{11}^{0E} = 28.83 \cdot 10^{10}$ dyn/cm², $c_{12}^{E0} = 11.4 \cdot 10^{10}$ dyn/cm², $c_{13}^{E0} = 42.87 \cdot 10^{10}$ dyn/cm², $c_{22}^{E0} = 26.67 \cdot 10^{10}$ dyn/cm², $c_{23}^{E0} = 14.5 \cdot 10^{10}$ dyn/cm², $c_{33}^{E0} = 65.45 \cdot 10^{10}$ dyn/cm², $c_{15}^{E0} = 5.13 \cdot 10^{10}$ dyn/cm², $c_{25}^{E0} = 8.4 \cdot 10^{10}$ dyn/cm², $c_{35}^{E0} = 7.50 \cdot 10^{10}$ dyn/cm², $c_{55}^{E0} = 5.20 \cdot 10^{10}$ dyn/cm².

The volume of a restricted primitive cell is $v = 0.467 \cdot 10^{-21}$ cm³ [7].

Now, let us dwell on the obtained results. The effect of hydrostatic pressure depend mainly on the behaviour of lattice strains u_j under pressure. Temperature dependence of these strains is presented in figure 2 by solid lines. In the paraelectric phase, they depend on temperature almost quadratically (dashed lines u_j^{para} in figure 2), in the temperature range $0 < T - T_c < 100$ K. Nonzero strains in the paraelectric

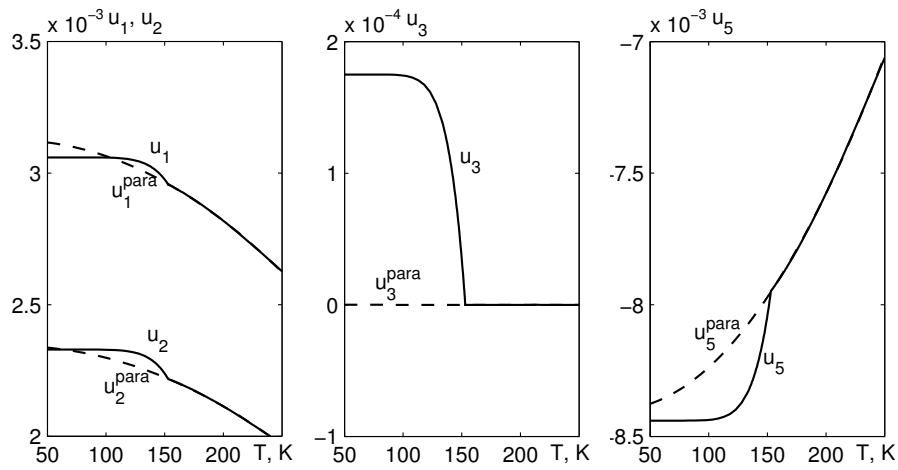


Figure 2. Temperature dependence of lattice strains u_j under zero pressure.

phase appear as a result of competition of energy of short-range interactions between pseudospins (2.3) [which depends on strains according to (2.4)] and elastic energy $Nv \frac{1}{2} \sum_{j,j'} c_{jj'}^{E0} u_j u_{j'}$ [see (2.2)]. They are an additional contribution to the thermal strains connected with anharmonicity of interatomic interactions, that was also noted earlier in [14]. In the ferroelectric phase the curves $u_j(T)$ deviate from the quadratic law owing to the appearance of spontaneous polarization. However, the curves $u_j(T)$ ($j = 1, 2, 5$) cannot be represented in the ferroelectric phase simply as a sum of u_j^{para} and of the item proportional to the spontaneous polarization, even roughly. Moreover, the differences $u_j - u_j^{\text{para}}$ ($j = 1, 2, 5$) change their sign at some temperature (figure 3), which qualitatively agree with experimental data [14].

The lattice strains u_j practically linearly depend on pressure according to Hooke's law. According to (2.4), (2.13), (2.14), this leads to a linear weakening under pressure of interaction parameters w , ν_1 , ν_2 , respectively. Here, in the range of pressure $0 \text{ GPa} < p < 0.6 \text{ GPa}$, the parameter of short-range interactions w decreases by 10% (from 657 K to 602 K), whereas the parameters of long-range interactions ν_1 , ν_2 decrease up to negative values (figure 4). Consequently, the phase transition temperature lowers (see figure 5, curve T_c). Such dependence $T_c(p)$ exists up to some critical pressure p_c . Here, the phase transition at the T_c point remains to be the second order transition, and the temperature dependences of different thermodynamic characteristics do not qualitatively change under pressure. In particular, spontaneous polarization monotonously and continuously decreases with an increasing temperature and tends to zero at the T_c point (figure 6, curves 1–4); dielectric permittivity ϵ_{22} tends to infinity at the temperature T_c (figure 7, curves 1–4). It is necessary to note that the theory concerns the monodomain crystal; it does not take into account reorientation of domain walls, which gives a large contribution to the experimentally measured permittivity in ferroelectric phase. Therefore, the permittivity ϵ_{22} does not agree with experimental data in ferroelectric phase. Temperature dependence of the proton contribution to molar heat capacity also does not qualitatively change under pressure (figure 8, curves 1–4). It has a jump at the T_c point, which slightly decreases with pressure. Total molar heat capacity (figure 9, solid line) is the sum of the proton contribution and the lattice contribution (dashed line) obtained in [19] using ab-initio calculations.

Longitudinal electric field E_2 smears the phase transition from paraelectric to ferroelectric phase. As a result, curves $P_2(T)$, $\epsilon_{22}(T)$ and $\Delta C_p(T)$ become smooth (see figures 10,11,12, respectively). In these figures, the field effect under zero pressure is demonstrated. Under nonzero values of pressure $p < p_c$, the field effect is similar.

As it is shown above, the constants of long-range interactions ν_1 and ν_2 linearly weaken with pressure. Starting from the critical pressure $p_c = 0.315 \text{ GPa}$ (experimental value is $p_c = 0.33 \pm 0.02 \text{ GPa}$), the parameter of “inter-sublattice” interactions ν_2 becomes negative (figure 4). Consequently, the sublattices “A” and “B” orient in opposite directions, and the crystal passes to antiferroelectric phase (curve T_N

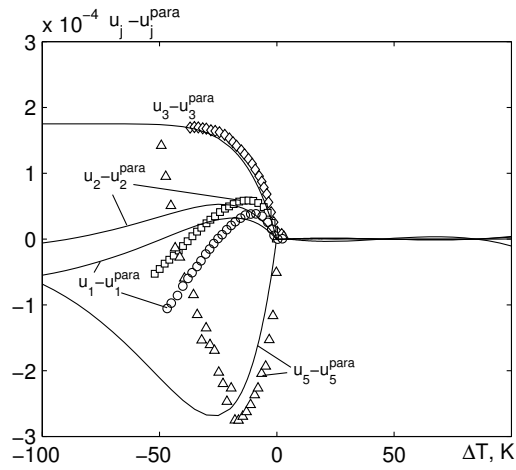


Figure 3. Temperature dependence of differences $u_j - u_j^{\text{para}}$ under zero pressure. Symbols are experimental data [14].

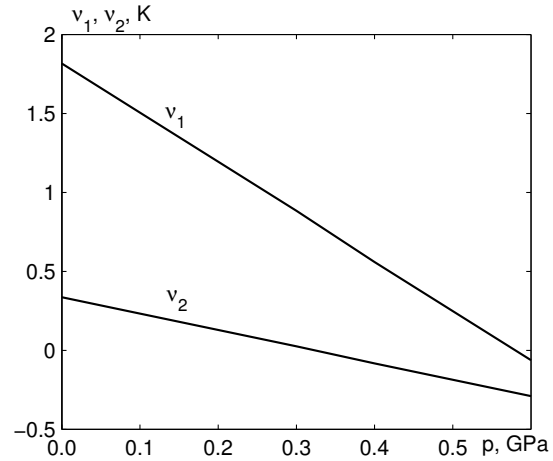


Figure 4. Pressure dependence of the parameters of long-range interactions v_1, v_2 at the temperature 80 K.

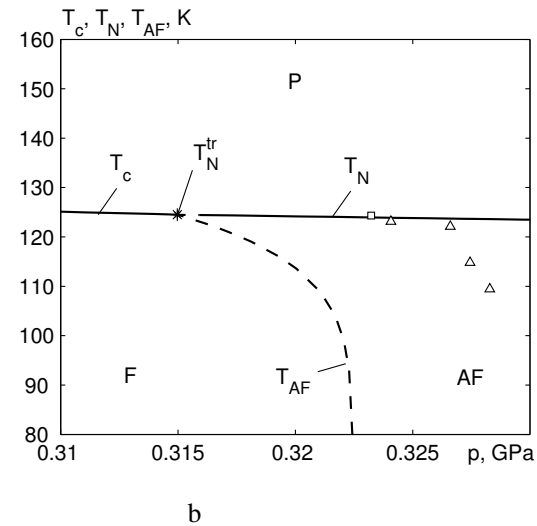
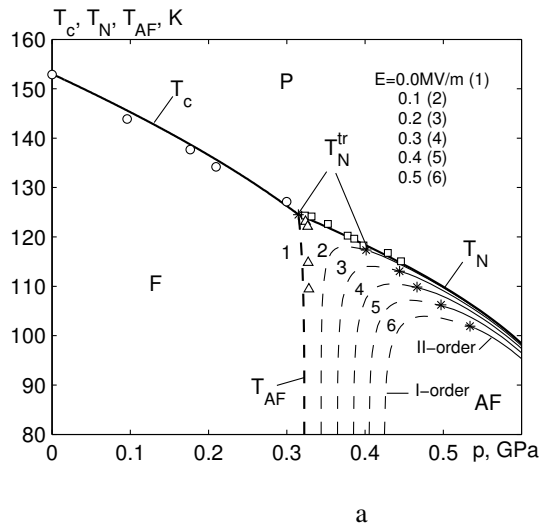


Figure 5. (a) Pressure dependence of the phase transition temperatures paraelectric-ferroelectric (T_c), paraelectric-antiferroelectric (T_N) and ferroelectric-antiferroelectric (T_{AF}) of CDP crystal at different values of the electric field E_2 (MV/m): 0.0 – 1, 0.1 – 2, 0.2 – 3, 0.3 – 4, 0.4 – 5, 0.5 – 6. Symbols are experimental data, taken from [5]. Tricritical points T_N^{tr} (denoted as *) separate the curves of first order (dashed lines) and second order (solid lines) phase transitions. (b) The same phase diagram, but near critical pressure.

in figure 5) instead of ferroelectric phase. Here, spontaneous polarization is absent, and longitudinal permittivity ε_{22} is finite and has a sharp band in the T_c point (figure 7, curves 5,6).

In the presence of electric field E_2 , the order parameter η_1 slightly increases, in comparison with the case of $E_2 = 0$ (figure 13, curves 1–6). The parameter η_2 , which is negative, on the contrary, decreases in value in comparison with the case of $E_2 = 0$ (figure 13, curves 1'–6'), moreover, a decrease in value of η_2 is stronger than an increase of η_1 . That is, in antiferroelectric phase at the presence of the field E_2 , the disordering of pseudospins in the sublattice “A” is stronger than the ordering in the sublattice “B”.

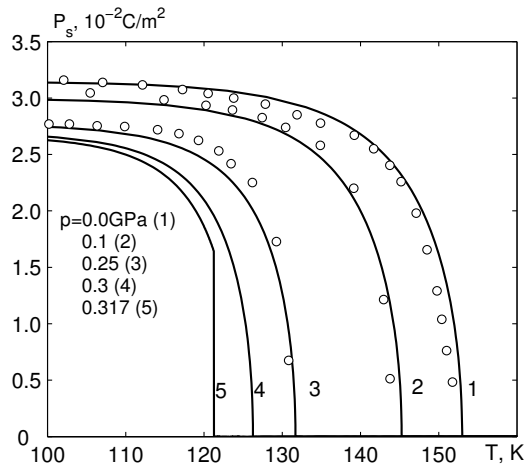


Figure 6. Temperature dependence of spontaneous polarization of CDP at different values of hydrostatic pressure p , GPa: 0.0 – 1, 0.1 – 2, 0.25 – 3, 0.3 – 4, 0.317 – 5. Symbols \circ are experimental data [5].

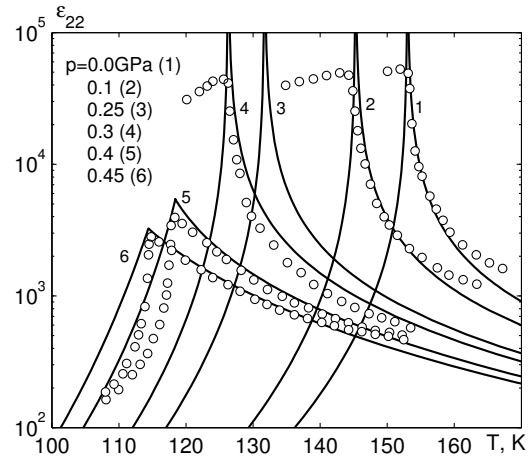


Figure 7. Temperature dependence of longitudinal dielectric permittivity of CDP at different values of hydrostatic pressure p , GPa: 0.0 – 1, 0.1 – 2, 0.25 – 3, 0.3 – 4, 0.4 – 5, 0.45 – 6. Symbols \circ are experimental data of [5].

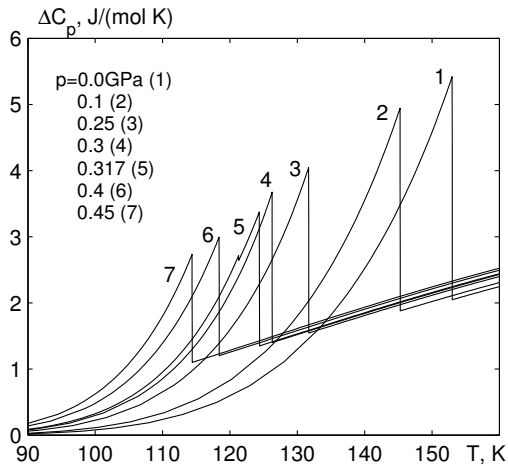


Figure 8. (Colour online) Temperature dependence of the proton contribution to molar heat capacity of CDP at different values of hydrostatic pressure p , GPa: 0.0 – 1, 0.1 – 2, 0.25 – 3, 0.3 – 4, 0.317 – 5, 0.4 – 6, 0.45 – 7.

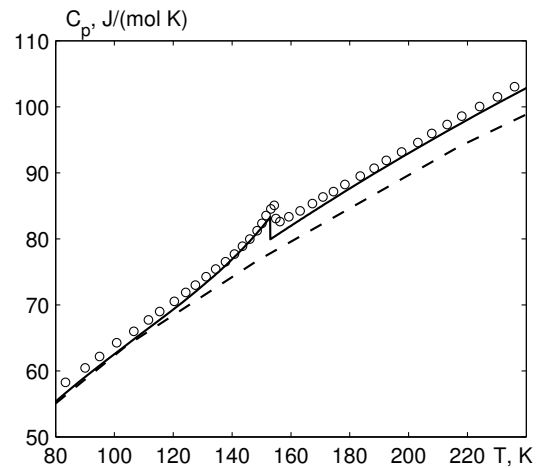


Figure 9. Temperature dependence of the total molar heat capacity of CDP. Symbols \circ are experimental data taken from [17], dashed line is a result of ab-initio calculations [19].

Consequently, in the antiferroelectric phase, dielectric permittivity increases in comparison with the case of $E_2 = 0$, and there appears a break at the T_N point on the curves $\varepsilon_{22}(T)$ (figure 14). Molar heat capacity also increases in the antiferroelectric phase in comparison with the case of $E_2 = 0$ (figure 15). Inasmuch as the field induces polarization P_2 above T_N point, then herein below the temperature region above T_N in the presence of the field will be referred to as “ferroelectric phase”. At some critical value of the field E_{cr} at constant values of pressure $p > p_c$ and temperature, the order parameter η_2 becomes positive, which means that there takes place an overturn of pseudospins in the sublattice “B”, and the crystal passes from antiferroelectric to ferroelectric phase. The calculated values of E_{cr} are several times larger in magnitude than the values experimentally measured in [6]. In particular, at $p = 0.38$ GPa at

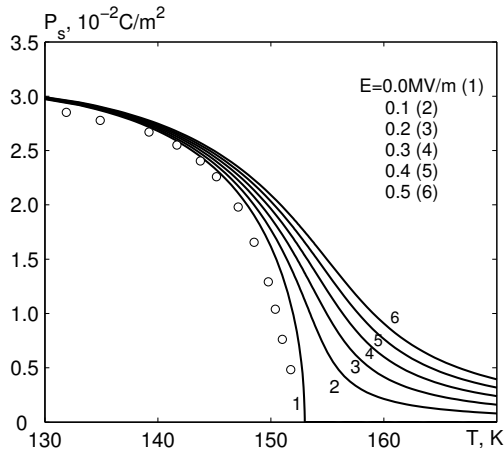


Figure 10. The temperature dependence of polarization of CDP crystal at $p=0$ GPa at different values of electric field E_2 (MV/m): 0.0 – 1, 0.1 – 2, 0.2 – 3, 0.3 – 4, 0.4 – 5, 0.5 – 6. Symbols \circ are experimental data [5].

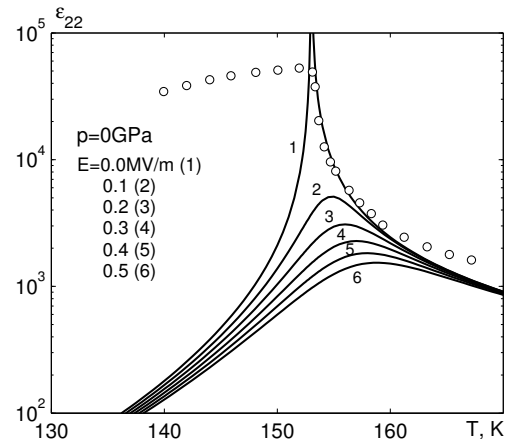


Figure 11. Temperature dependence of dielectric permittivity of CDP crystal at $p=0$ GPa at different values of electric field E_2 (MV/m): 0.0 – 1, 0.1 – 2, 0.2 – 3, 0.3 – 4, 0.4 – 5, 0.5 – 6. Symbols \circ are experimental data [5].

low temperatures $E_{cr} \approx 0.28$ MV/m, whereas the experimental value is $E_{cr} \approx 0.06$ MV/m. That is, the present model only qualitatively describes the field effect.

Disagreement of the calculated E_{cr} with experimental data can be explained in such a way. In expression (2.27), the terms, that describe the interaction of a pseudospin with external field $1/2\beta(\mu_y E_2)$ and with the other sublattice $\beta v_2 \eta_1$, have opposite signs (because at $p > p_c$ parameter $v_2 < 0$), which means that they compete with each other. At the field $E > E_{cr}$, the interaction with external field prevails, and the order parameter η_2 changes its sign to the opposite. In order to obtain the value of $\mu_y E_2$ large enough to turnover the pseudospin, at the weaker field, the dipole moment μ_y should be larger. On the other hand, μ_y cannot be larger, because it fixes the saturation polarization, inasmuch as polarization depends mainly on the product $\mu_y(\eta_1 + \eta_2)$ [see (3.3), but the order parameters $\eta_1, \eta_2 \rightarrow 1$ when $T \rightarrow 0$].

However, if we took into account the tunneling of protons on the hydrogen bonds, then the order

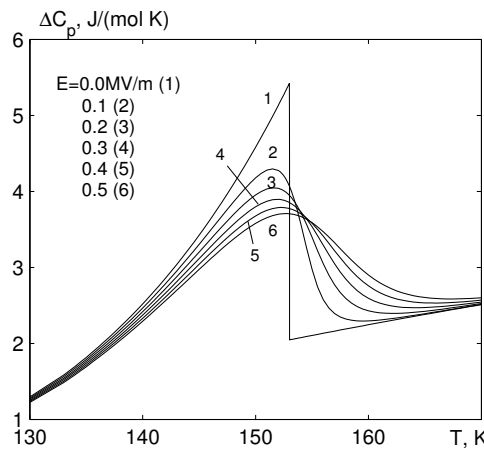


Figure 12. Temperature dependence of the proton contribution to molar heat capacity of CDP at $p = 0$ GPa at different values of electric field E_2 (MV/m): 0.0 – 1, 0.1 – 2, 0.2 – 3, 0.3 – 4, 0.4 – 5, 0.5 – 6.

parameters would be $\eta_1, \eta_2 < 1$ at $T \rightarrow 0$. That is why the parameter μ_y in this case would be larger than without taking into account the tunneling. Strong isotopic effect in the CDP may be the evidence of tunneling effects. Besides, the distribution function of the proton momentum, obtained by ab-initio calculations in [21], has an additional peak at nonzero momentum at low temperatures, which points to a tunneling effect. It is also shown in [21], that the shortening of the hydrogen bond with double-well potential by 1% lowers the energy barrier between the equilibrium positions several times. As a result, the tunneling effect on these bonds would greatly increase with pressure. Hence, the disagreement of E_{cr} with the experimental data is connected, to a great extent, with neglecting the proton tunneling processes in the present model.

As a consequence of turnover of pseudospins at the presence of the external field at a constant pressure, the temperature T_N lowers approximately by the law $T_N \sim -E_2^2$ (figure 16). The lowering of T_N

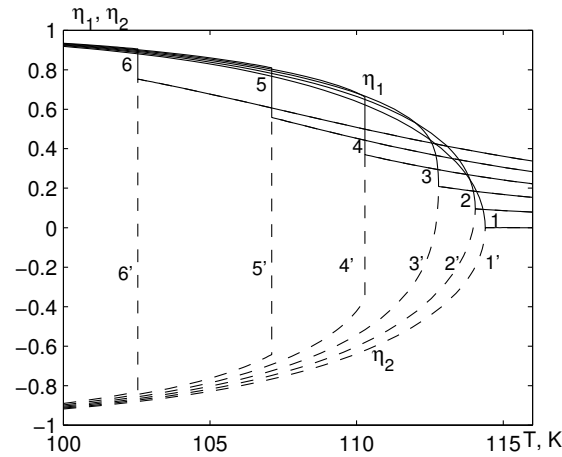


Figure 13. Temperature dependences of the order parameters η_1 (solid lines) and η_2 (dashed lines) at $p = 0.45$ GPa at different values of electric field E_2 (MV/m): 0.0 – 1, 0.1 – 2, 0.2 – 3, 0.3 – 4, 0.4 – 5, 0.5 – 6.

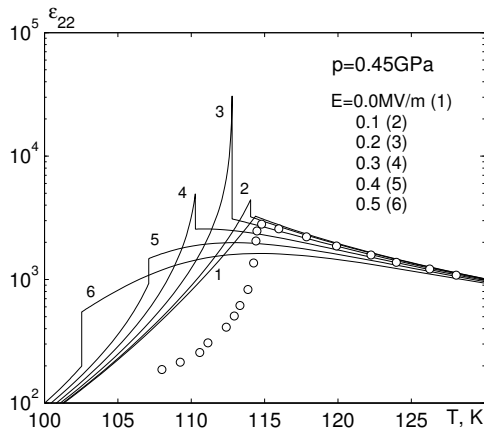


Figure 14. Temperature dependence of dielectric permittivity of CDP crystal at $p = 0.45$ GPa at different values of electric field E_2 (MV/m): 0.0 – 1, 0.1 – 2, 0.2 – 3, 0.3 – 4, 0.4 – 5, 0.5 – 6. Symbols \circ are experimental data [5].

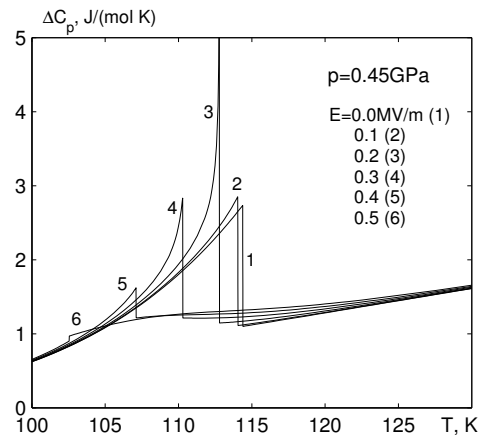


Figure 15. Temperature dependence of the proton contribution to molar heat capacity of CDP crystal at $p = 0.45$ GPa at different values of electric field E_2 (MV/m): 0.0 – 1, 0.1 – 2, 0.2 – 3, 0.3 – 4, 0.4 – 5, 0.5 – 6.

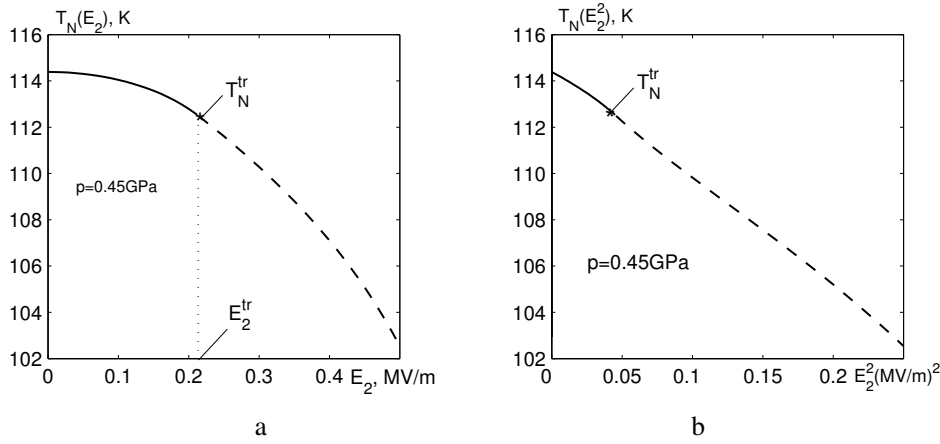


Figure 16. Dependence of temperature T_N on electric field E_2 (a) and on square of the field (b) at $p = 0.45$ GPa. Tricritical points T_N^{tr} separate the curves of first order (dashed lines) and second order (solid lines) phase transitions.

also reveals itself in the shift of the break on curves $\varepsilon_{22}(T)$ to lower temperatures (figure 14), as well as in the suppression of the antiferroelectric region (AF) on the phase diagram (see figure 5, curves 2–6). As one can see from figure 5, the closer is the value of hydrostatic pressure to the critical value p_c , the stronger is the effect of the field E_2 on the temperature T_N .

It is necessary to note that in weak fields, the phase transition in the T_N point remains the second order phase transition (solid lines in figure 16 and in figure 5, curves 2–6), but starting from some value of the field E_2^{tr} (tricritical point) it becomes a first order phase transition (dashed lines in figure 16 and in figure 5, curves 2–6).

The above mentioned increase of permittivity in antiferroelectric phase in comparison with the case of $E_2 = 0$ takes place at fields $E_2 < E_2^{\text{tr}}$ (figure 14, curves 2, 3). At the fields $E_2 > E_2^{\text{tr}}$, the permittivity ε_{22} decreases again (figure 14, curves 4–6), because the order parameters η_1, η_2 in antiferroelectric phase near T_N temperature become closer to saturation at a further strengthening of the field (see figure 13, curves 4, 4', 5, 5', 6, 6').

Let us investigate the behavior of thermodynamic characteristics under pressures close to the critical: $p = 0.315 \div 0.322$ GPa. Dependence of the lattice strains on temperature $u_j(T)$ reveals itself especially strongly under such pressures. Namely, the parameter of inter-sublattice interactions ν_2 changes its sign with the lowering of temperature. As a result, at a constant pressure, the crystal passes firstly from paraelectric to antiferroelectric phase at the temperature T_N , and with a further lowering of temperature it passes from antiferroelectric to ferroelectric phase at some temperature T_{AF} , as one can see in figure 5, b. Here, the phase transition at the T_{AF} point is the first order. In particular, at $p = 0.317$ GPa, the spontaneous polarization exists under temperature $T_{\text{AF}} = 121.3$ K (figure 6, curve 5), the temperature dependence of the proton contribution to the heat capacity ΔC_p has breaks at temperatures $T_N = 124.4$ K and $T_{\text{AF}} = 121.3$ K (see figure 8, curve 5), and the temperature dependence of dielectric permittivity ε_{22} has a sharp band at the T_N point and a small break at the T_{AF} point (see figure 17). As one can see from this figure, the agreement of theory with experimental data is only qualitative. Probably, the properties of CDP near the critical pressure p_c strongly depend on the quality of a sample. It is necessary to note that when the temperature lowers the theoretical curve ε_{22} has a jump down in the T_{AF} point, whereas the experimental values of ε_{22} , on the contrary, abruptly increase due to the contribution to permittivity from reorientation of domain walls.

Near the critical pressure, the properties of a crystal are very sensitive to the electric field. From the temperature dependence of polarization at $p = 0.317$ GPa (see figure 18) one can see that weak fields (up to 2 kV/m) greatly increase the temperature T_{AF} and greatly lower the temperature T_N . Here, in the external field the temperature position of the break on the curves of dielectric permittivity and heat capacity at T_{AF} point shifts to the higher temperatures, whereas the effect of the field on the thermodynamic characteristics

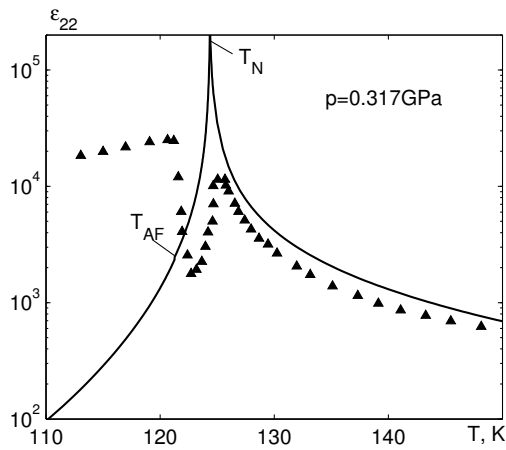


Figure 17. Temperature dependence of longitudinal dielectric permittivity of CDP at $p = 0.317$ GPa. Symbols \blacktriangle are experimental data [5].

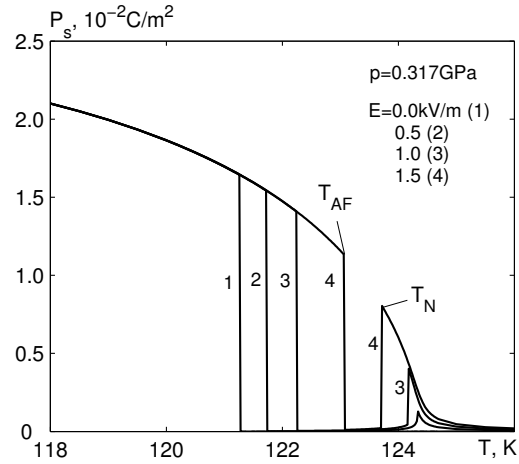


Figure 18. Temperature dependence of polarization of CDP at $p = 0.317$ GPa at different values of electric field E_2 (kV/m): 0.0 – 1, 1.0 – 2, 2.0 – 3, 3.0 – 4.

near T_N point at $p = 0.317$ GPa is qualitatively similar to the case of $p = 0.45$ GPa. Consequently, at a constant pressure, the electric field E_2 decreases the temperature range, at which the antiferroelectric phase exists, up to its complete disappearance, and at a constant temperature this field increases the critical pressure (see figure 5, curves 2–6).

5. Conclusions

The lowering of the phase transition temperature T_c with pressure is connected with the weakening of long-range and short-range (to a lesser extent) interactions. Under the pressures higher than some critical pressure p_c , the inter-sublattice interactions become negative. Consequently, there appear paraelectric-antiferroelectric and ferroelectric-antiferroelectric phase transitions.

The dependence of the lattice strains (as well as long-range interactions) on temperature reveals itself mainly near the critical pressure. Namely, the inter-sublattice interactions change their sign with the lowering of temperature. As a result, at a constant pressure, close to the critical pressure, the crystal passes first from paraelectric to antiferroelectric phase, and with a further lowering of temperature it passes from antiferroelectric to ferroelectric phase.

Longitudinal electric field E_2 increases the critical pressure. Under pressures $p < p_c$, the external field smears the phase transition. Under pressures $p > p_c$, the external field lowers the temperature T_N and increases the permittivity ϵ_{22} in the antiferroelectric phase. This can be explained by a larger disordering of pseudospins in the sublattice “B” than the ordering in the sublattice “A” in the presence of the electric field. A strong enough field can change the order of phase transition at the T_N point from second order to first order. The strongest field effect on the calculated characteristics takes place near the critical pressure.

References

1. Matsunaga H., Itoh K., Nakamura E., J. Phys. Soc. Jpn., 1980, **48**, No. 6, 2011–2014, doi:10.1143/JPSJ.48.2011.
2. Itoh K., Hagiwara T., Nakamura E., J. Phys. Soc. Jpn., 1983, **52**, No. 8, 2626–2629, doi:10.1143/JPSJ.52.2626.
3. Iwata Y., Koyano N., Shibuya I., J. Phys. Soc. Jpn., 1980, **49**, No. 1, 304–307, doi:10.1143/JPSJ.49.304.
4. Iwata Y., Deguchi K., Mitani S., Shibuya I., Onodera Y., Nakamura E., J. Phys. Soc. Jpn., 1994, **63**, No. 11, 4044–4050, doi:10.1143/JPSJ.63.4044.
5. Yasuda N., Okamoto M., Shimizu H., Fujimoto S., Yoshino K., Inuishi Y., Phys. Rev. Lett., 1978, **41**, No. 19, 1311–1314, doi:10.1103/PhysRevLett.41.1311.

6. Yasuda N., Fujimoto S., Okamoto M., Shimizu H., Yoshino K., Inuishi Y., Phys. Rev. B., 1979, **20**, No. 7, 2755–2764, doi:10.1103/PhysRevB.20.2755.
7. Schuele P.J., Thoma R.A., Jpn. J. Appl. Phys., 1985, **24**, 935–937, doi:10.7567/JJAPS.24S2.935.
8. Schuele P.J., Schmidt V.H., Phys. Rev. B., 1989, **39**, No. 4, 2549–2556, doi:10.1103/PhysRevB.39.2549.
9. Kobayashi Yu., Deguchi K., Azuma Sh., Suzuki E., Ming Li Ch., Endo Sh., Kikegawad T., Ferroelectrics, 2003, **285**, No. 7, 83–89, doi:10.1080/00150190390205924.
10. Brandt N.B., Zhukov S.G., Kulbachinskii V.A., Smirnov P.S., Strukov B.A., Fiz. Tverd. Tela, 1986, **28**, 3159, (in Russian).
11. Magome E., Tomiaka S., Tao Y., Komukae M., J. Phys. Soc Jpn., 2010, **79**, No. 2, 025002, doi:10.1143/JPSJ.79.025002.
12. Blinc R., SaBaretto F.C., J. Chem. Phys., 1980, **72**, No. 11, 6031–6034, doi:10.1063/1.439058.
13. Stasyuk I.V., Levytsky R.R., Zachek I.R., Shchur Ya.Y., Kutny J.V., Miz E.V., Preprint of the Institute for Condensed Matter Physics, ICMP–91–4R, Lviv, 1991, (in Russian).
14. Deguchi K., Okaue E., Ushio S., Nakamura E., Abe K., J. Phys. Soc. Jpn, 1984, **53**, No. 9, 3074–3080, doi:10.1143/JPSJ.53.3074.
15. Levitskii R.R., Zachek I.R., Vdovych A.S. Phys. Chem. Solid State, 2012, **13**, No. 1, 40–47.
16. Levitskii R.R., Zachek I.R., Vdovych A.S., J. Phys. Stud., 2012, **16**, No. 4, 4702 (in Ukrainian).
17. Imai K., J. Phys. Soc. Jpn., 1983, **52**, No. 11, 3960–3965, doi:10.1143/JPSJ.52.3960.
18. Prager S., Smith T.F., Finlayson T.R., Aust. J. Phys., 1985, **38**, No. 1, 63–83, doi:10.1071/PH850063.
19. Shchur Ya., Bryk T., Klevets I., Kityk A.V., Comput. Mater. Sci., 2016, **111**, 301–309, doi:10.1016/j.commatsci.2015.09.014.
20. Van Troeye B., van Setten M.J., Giantomassi M., Torrent M., Rignanese G.-M., Gonze X., Phys. Rev. B., 2017, **95**, No. 2, 024112, doi:10.1103/PhysRevB.95.024112.
21. Lasave J., Abufager P., Koval S., Phys. Rev. B, 2016, **93**, No. 13, 134112, doi:10.1103/PhysRevB.93.134112.

Вплив гідростатичного тиску та поздовжнього електричного поля на фазові переходи та термодинамічні характеристики квазіодновимірної сегнетоелектрика CsH_2PO_4

А.С. Вдович ¹, І.Р. Зачек ², Р.Р. Левицький ¹

¹ Інститут фізики конденсованих систем НАН України, вул. Свенціцького, 1, 79011 Львів, Україна

² Національний університет “Львівська політехніка”, вул. С. Бандери, 12, 79013 Львів, Україна

Запропоновано двопідграткову модель протонного впорядкування квазіодновимірної сегнетоелектрика з водневими зв'язками CsH_2PO_4 , яка враховує лінійні за деформаціями ґратки u_1 , u_2 , u_3 і u_5 внески в енергію протонної підсистеми. Модель враховує також залежність ефективних дипольних моментів псевдоспінів від параметрів впорядкування, що дозволяє узгодити ефективні дипольні моменти в сегнето- і парафазі. У рамках цієї моделі в наближенні двочастинкового кластера за короткосяжними і середнього поля за далекосяжними взаємодіями, досліджено поведінку спонтанної поляризації, поздовжньої діелектричної проникності і молярної теплоємності під дією гідростатичного тиску і поздовжнього електричного поля. Пояснено перехід в антисегнетофазу при високих тисках. Вивчено характер розмиття фазового переходу парафаза-сегнетофаза, а також пригнічення антисегнетофази в електричному полі.

Ключові слова: сегнетоелектрики, діелектрична проникність, фазові переходи, вплив гідростатичного тиску, вплив електричного поля